Krzysztof J. OPIELIŃSKI[1], Piotr PRUCHNICKI[2]

12. ANALYSIS OF THE POSSIBILITY OF USING CODED PULSES IN ULTRASOUND TOMOGRAPHY

12.1. Introduction

In echo imaging, significant improvement in the detection of pathological changes in tissue structure can be achieved by increasing the signal-to-noise (S/N) ratio of received ultrasound echoes [1, 2]. At a certain level of receiver noise, this requires an increase in signal energy, which can be achieved by increasing the length of transmitting pulses, as their amplitude is limited by the acceptable power that can be used in conventional ultrasound echo imaging.

In turn, from the point of view of improving the resolution of ultrasound echo imaging, the echo pulses reflected from heterogeneity in tissue structure should be as short as possible. It is assumed that the minimum distinguishable distance ΔR between adjacent ultrasound imaging structures (range resolution):

$$\Delta R \leq \frac{c}{2B}, \tag{1}$$

where c – the speed of ultrasonic wave propagation in the tissue, B – frequency range of ultrasonic array transducers. This condition can be interpreted in such a way that the pulse duration should be correspondingly shorter than the time the ultrasound wave passes between adjacent structures imaged by ultrasounds. In this way, the received echo pulses will be appropriately separated from each other in time. The simultaneous provision by the conventional ultrasound B-mode system of the best differentiation and detectability of objects leads to opposite requirements for the probing signal, because the longer the transmitting (sending) signal is, the better the detectability, while the resolution is better the shorter the

[1] Department of Acoustics, Multimedia and Signal Processing, Wroclaw University of Science and Technology, Wyb. Wyspiańskiego 27, 50-370 Wrocław, Poland,
DRAMIŃSKI S.A., Owocowa 17, 10-860 Olsztyn, Poland, krzysztof.opielinski@pwr.edu.pl
[2] Department of Acoustics, Multimedia and Signal Processing, Wroclaw University of Science and Technology, Wyb. Wyspiańskiego 27, 50-370 Wrocław, Poland,
DRAMIŃSKI S.A., Owocowa 17, 10-860 Olsztyn, Poland, piotr.pruchnicki@pwr.edu.pl

echoes are. The effect of maximum peak power on the ratio of examination depth to desired range resolution in ultrasonic reflection methods can be expressed using the formula [3, 4]:

$$\frac{R}{\Delta R} \leq f_{\text{rep}} \cdot t_{\text{pulse}} = \frac{P_{\text{peak}}}{P_{\text{avg}}}, \tag{2}$$

where R – the range of examination, ΔR – range (axial) resolution, f_{rep} – pulse repetition rate, t_{pulse} – pulse duration, P_{peak} – peak power, P_{avg} – average power. This problem of ensuring the best differentiation and detection of objects by the ultrasound B-mode system at the same time can therefore be solved by using specially selected long sequences of transmitting signals, which would enable the compression of returning echoes using appropriately matched filters or employing echo correlation with the replica of the transmitting sequence [5]. As a result, no large peak power will be required to improve the signal-to-noise ratio.

In ultrasound coded transmission, signals with linear frequency modulation (so-called chirp) and discrete phase modulation with algebraic codes (Barker codes, Golay codes) are used (adapted from radar technique) [1, 2]. In all such solutions, echoes are correlated with the standard transmission signal and then averaged. In this way, a large amplitude of the sounding signals is not required, because the gain in the signal-to-noise ratio results from the compression of the recorded echoes.

Linear frequency modulation with a chirp signal is characterized by the presence of side lobes with a level of about -13 dB in relation to the main lobe, which prevents good quality imaging. Lowering the level of the side lobes to about -40 dB can be achieved by using window methods. The advantage of chirp codes is their resistance to frequency changes and the possibility of shaping the frequency band, which allows for the proper selection of the signal to the ultrasonic array band. Golay codes are characterized by a lack of side lobes and the gain proportional to the number of bits of the sending code. Depending on the type of changes in signal characteristics over time, coded signals can be divided into continuous and discrete [1]. There are 3 basic methods of continuous (analog) modulation:

1) AM - amplitude modulation,
2) FM - frequency modulation,
3) PM - phase modulation

and 3 methods of discreet (digital) modulation respectively:

1) ASK - amplitude shift keying,
2) FSK - frequency shift keying,
3) PSK - phase shift keying.

The most commonly used method of continuous modulation is linear frequency modulation (FM) using the chirp signal. The most commonly used discrete modulation method is phase shift keying (PSK) using Golay and Barker binary codes. Based on the results presented in the literature [6-8], it can be concluded that ultrasound-coded transmission provides improved image quality and increased S/N ratio values, with the best results being obtained when using

complementary Golay codes, due to the significant minimization of lateral lobes and a significant reduction in pulse duration as a result of matched filtering.

Coded signals can also be attempted to improve imaging quality in ultrasound transmission and reflection tomography [9], similarly to ultrasound echo imaging. However, it is difficult to find references on such applications. The authors most often focus on signal studies [10], because the use of computerized tomography (CT) image reconstruction requires the development of special algorithms for the detection of transition time and pulse amplitude in the case of transmission, and pulse amplitude in the case of reflective signals. For this purpose, additional examinations are necessary due to the side lobes of the signals obtained from the emission of coded pulses. In the case of ultrasound transmission tomography scans, there occurs a multitude of pulse transitions in the heterogeneous structure of the glandular breast tissue, which are transmitted with different refractions that overlap with the shifted phases. This phenomenon results in uncontrolled elongation and flattening of the envelope of the pulses transmitted through the breast structure, which complicates the precise determination of the transition time. In the case of reflective signals, the side lobes cause uncontrolled shifting of the maximum echo envelope. Transmission tests with the use of coded pulses are usually carried out in a water tank, in which a single ultrasonic transmitter powered from a programmable pulse generator is immersed [10]. In the same tank, at a fixed distance from the surface of the transmitter, a hydrophone is located, which can rotate around the circle on which the transmitter is located. Such a measuring system refers to the divergent scanning geometry used in ultrasound tomography using an array of ultrasonic transducers located on the inside of the ring. Results of such transmission tests show that the use of transmission signal coding does not limit the angle of divergence of the transducer beam, which in the case of ultrasound tomography should be as wide as possible. In the case of imaging of strongly suppressing structures, such as breast gland tissue, the highest S/N ratio values can be obtained using Golay and Barker codes compared to the use of short uncoded transmission pulses [10].

In this paper, the research using coded signals in the ultrasound transmission (UTT) and reflection tomography (URT) method was carried out on the model of ultrasound tomography developed by DRAMIŃSKI S.A. company in cooperation with a team of scientists from Wroclaw University of Science and Technology [9, 11]. The ultrasound tomography device was equipped with a special ultrasonic ring array consisting of 1024 elementary piezoceramic transducers (0.5 mm x 18 mm in size), evenly distributed on the inner side of the ring with 260 mm diameter [9, 12].

12.2. Materials and Methods

12.2.1. Measuring system

The modified setup of the ultrasound tomography model shown schematically in Fig. 1 was used for measurement purposes. This setup enables scanning of cross-sections of objects immersed in water in divergent geometry, in ultrasound transmission and reflection tomography modes. The measurements carried out in this work were performed using one of the first models of the UGP-2 ultrasonic ring array with the following transducer parameters: resonant frequency f_r = 1.96 MHz, frequency range B = 0.25 MHz, mechanical quality factor $Q \approx 8$. The digital infinite pulse response bandpass filter (FIR), which cuts out all recorded signals in the frequency range outside the 1.5 - 3.5 MHz was implemented in the measurement data acquisition software.

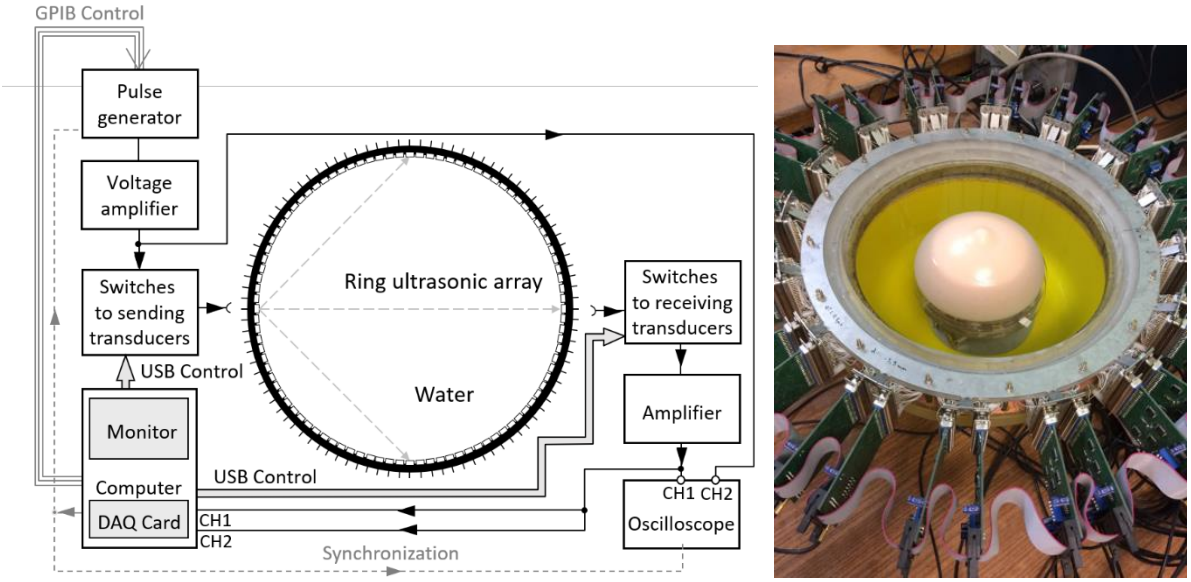

Fig. 1. The modified measuring setup of the ultrasound tomography model (diagram and photo)
Rys. 1. Zmodyfikowany układ pomiarowy modelu tomografu ultradźwiękowego (schemat blokowy i fotografia)

12.2.2. Normal and coded pulses

The pulse generator (AFG 3022) in the measuring system (Fig. 1) has been programmed in such a way that it is possible to load into its memory and generate arbitrary pulses (of a given shape) sequentially. The programmed pulses were used as pulses powered the transmitter (or transmitter-receiver) of the ultrasound tomography ring array. There were 5 types of arbitrary pulses programmed, the shape of which is shown in Fig. 2.

A single period of arbitrary pulses was selected so that the frequency of their filling was adjusted to the resonance frequency $f_r \approx 2$ MHz of elementary piezoceramic transducers of the

ring array. A 5-period symmetrical rectangular pulse with 100% duty cycle (Fig. 2a) was selected as the uncoded signal (so-called normal signal). The chirp signal with linear frequency modulation (Fig. 2b) is a signal in which the temporary frequency $f_i(t)$ changes linearly with time, starting from the frequency $f = f_0 - B$ at the time instant $t = t_0 - T/2$ to the frequency after time $t = t_0 + T/2$ [2, 13], according to the formula:

$$s(t) = \mathrm{rect}\left(\frac{2t-T}{2T}\right) \cdot \cos\left(2\pi\left(f_0 \cdot \left(t - \frac{T}{2}\right) + \frac{B}{2T}\left(t - \frac{T}{2}\right)^2\right)\right), \tag{3}$$

where f_0 − the central frequency of the signal, B - the band around the central frequency, T – the designed duration of the chirp pulse (in a rectangular time window with a unit amplitude), $t_0 = T/2$, rect – the function of the rectangular window. For testing, a 12-period chirp sine wave forming symmetrical pulse with linear frequency modulation in the range 1 − 3 MHz was selected and programmed (Fig. 2b).

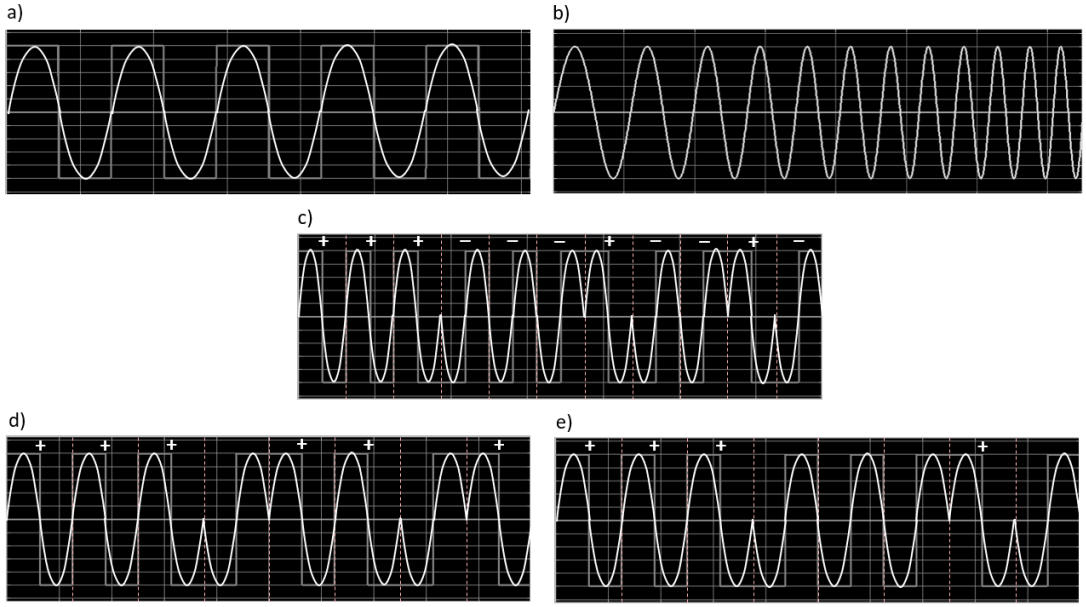

Fig. 2. Programmed arbitrary pulses: a) 5-period sine wave forming symmetrical pulse with 100% duty cycle, b) 12-period chirp sine wave forming symmetrical pulse with linear frequency modulation in the range of 1 - 3 MHz, c) 11-bit Barker's pulse phase-keyed, d) 8-bit Golay's pulse phase-keyed - A (first) from complementary pair, e) 8-bit Golay's pulse phase-keyed - B (second) from complementary pair

Rys. 2. Zaprogramowane impulsy arbitralne: a) 5-okresowy symetryczny impuls sinusoidalny z wypełnieniem 100%, b) 12-okresowy symetryczny impuls sinusoidalny typu *chirp* z liniową modulacją częstotliwości w zakresie 1 - 3 MHz, c) 11-bitowy impuls Barkera kluczowany fazowo, d) 8-bitowy impuls Golaya kluczowany fazowo - A (pierwszy) z pary komplementarnej, e) 8-bitowy impuls Golaya kluczowany fazowo - B (drugi) z pary komplementarnej

The Barker code (Fig. 2c) belongs to the signals encoded with biphasic modulation [2, 10]. The Barker code is included in the so-called optimal codes because the structure of the side lobes of the coded pulse contains the minimum theoretically possible energy, which is uniformly distributed between the lobes. The amplitude of the side lobes is the inverse of the length of the N code at the output signal normalized to 1. The compression ratio is proportional to the length of the N code so that each additional element of the code increases the compression ratio by 1. In practical applications, algebraic codes are not transmitted directly but modulate (key) the amplitude, phase, or frequency of the carrier signal binary. Most often the phase of the probe signal is keyed in this way by inverting it. The Barker code (Fig. 2c) with the length $N = 11$ and elements (+ + + – – – + – – + –) was selected and programmed for testing. The ratio of the maximum amplitude of the side lobes to the main lobe (PSL - Peak-to-Sidelobe Level) of this code is -20.8 dB and the ratio of the total energy of the side lobes to the energy of the main lobe (ISL - Integrated Sidelobe Level) is -10.8 dB.

Golay codes (Fig. 2d, Fig. 2e) belong to a wide class of complementary algebraic codes [14]. Complementary codes consist of a pair of codes of N length, whose autocorrelation functions have side lobes of the same value, but their signs are opposite. Thus, the sum of autocorrelation functions has a main lobe with an amplitude of $2N$ and is characterized by a total absence of side lobes [6]. For testing, a pair of complementary Golay codes of $N = 8$ length and elements (+ + + – + + – +) for code A and (+ + + – – – + –) for code B respectively were selected and programmed. The maximum value of the main lobe amplitude for this code pair is 16 dB.

12.2.3. Matched filtering

The essence of ultrasonic coded transmission is an appropriate correlation of the receiving signal with the reference transmission signal. For this purpose it is necessary to know the emitted signal because the signal of compressed pulses $R(\tau)$ is reconstructed from the received pulses $e(t)$ by correlating it with the signal $s(t+\tau)$, which is the same as the emitted signal but shifted in time by τ, and is called a matching filter:

$$R(\tau) = \int_{-\infty}^{+\infty} e(t) \cdot s(t+\tau)\,\mathrm{d}t\,. \tag{4}$$

This type of matched filtering of the receiving signal was performed in the case of using the uncoded burst pulse (Fig. 2a) and chirp pulse (Fig. 2b) as the transmitting signal.

The transmitting and receiving process and the signal compression process in the case of using the Barker code as the transmitting signal was carried out according to the following scheme:

1) sending the Barker code,
2) reception of a signal for Barker code,

3) correlation of the signal of received pulses with the matched filter - a phase-keyed signal through a binary code inverse to the code in the transmission signal.

Instead of correlating the received signal with the matched filter, we can perform the convolution operation directly with the transmitted Barker code. Fig. 3 shows the comparison of the signal obtained from the matched filter (correlation) of the 5-period Barker code with the pulse obtained from the matched filter (autocorrelation) of the 5-period uncoded sine wave burst [1]. In both cases presented in Fig. 3, the amplitude of the pulses after the matched filtering is 5 times higher than that of the transmitting pulse. The ISL ratio increases by 8 dB, but the level of the side lobes when using Barker codes (-14 dB, Fig. 3b) is much lower compared to the uncoded string (-1.9 dB, Fig. 3a), which shows the significant benefit of using Barker code [1].

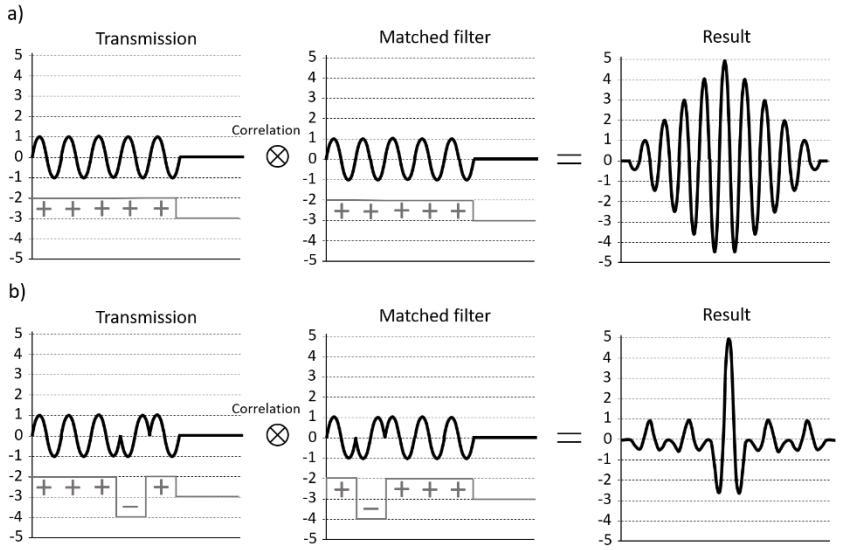

Fig. 3. Comparison of the pulse obtained from the matched filtering (autocorrelation) of the 5-period sine waveform (a) with the pulse obtained from the matched filtering (correlation) of the 5-period Barker code (b) [1]

Rys. 3. Porównanie impulsu uzyskanego w wyniku filtracji dopasowanej (autokorelacji) 5-okresowego wycinka sygnału sinusoidalnego (a) z impulsem uzyskanym w wyniku filtracji dopasowanej (korelacji) 5-okresowego kodu Barkera (b) [1]

The transmitting and receiving process and the signal compression process in the case of using complementary Golay codes as transmitting signals followed the scheme:

1) sending the Golay A code (first of the complementary pair of codes),
2) receiving the signal for the Golay A code,
3) sending the Golay B code (the second of a complementary pair of codes),
4) receiving a signal for Golay B code,
5) convolution of the receiving signal for the Golay A code with the matched filter - transmitting signal keyed with Golay A code,

6) convolution the receiving signal for the Golay B code with the matched filter - transmitting signal keyed with Golay B code,
7) summing up the results of both convolutions for Golay A and B codes.

In the process of matched filtering the receiving signals for complementary Golay A and B codes, we can perform the convolution operation directly with the transmitted Golay signals instead of correlating them with the signals reversed in time. The use of correlation with the matched filter allows the use of programmable filters for this purpose, which can be implemented in FPGA electronics. On the other hand, the use of convolution operation allows for quick realization of this operation in digital circuits in the Fourier domain by multiplying the FFT transforms [7] (Fig. 4).

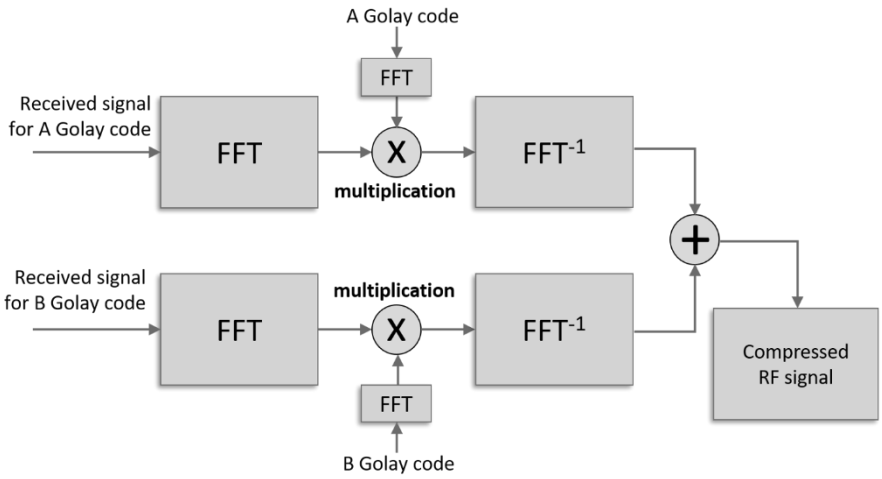

Fig. 4. Block diagram of the Golay code compression algorithm in the frequency domain
Rys. 4. Schemat blokowy algorytmu kompresji kodów Golaya w dziedzinie częstotliwości

The effectiveness of compression of the coded receiving signals depends on the transmitter-receiver setup bandwidth, which in practice comes down to the bandwidth of the ultrasonic array used [1]. As the band of the Golay sequence is reduced, the amplitudes of the receiving pulses decrease and their width increases significantly, which leads to a deterioration of imaging resolution.

12.2.4. Phantoms and objects studied

The measurements in the setup of the ultrasound tomography model (Fig. 1) were carried out for distilled water and the following phantoms and objects immersed in distilled water: a specially developed cylindrical agar gel phantom with three holes of different diameters filled with water, the Kyoto Kagaku Model US-9 Transparent Biopsy Breast Phantom [15], the CIRS

Model 052A Biopsy Breast Phantom [12], a wire test object [12]. Figure 5 shows the tested phantoms and objects.

The cylindrical agar phantom was chosen because of low ultrasound attenuation in agar gel and its shape suited for scanning in divergent tomographic geometry. Breast phantoms were selected because of the differential ultrasound attenuation in the gel structure (CIRS Biopsy Breast Phantom Model 052A - low attenuation, Kyoto Kagaku Biopsy Breast Phantom Model US-9 Transparent - high attenuation). The wire testing object was chosen because of the high ultrasound scattering factor on metal elements.

Fig. 5. Measured phantoms and objects, successively: cylindrical agar gel phantom, Kyoto Kagaku Model US-9 Transparent breast biopsy phantom [15], CIRS Model 052A breast biopsy phantom [12], wire testing object [12]

Rys. 5. Mierzone fantomy i obiekty, kolejno: walcowy fantom agarowy, biopsyjny fantom piersi Kyoto Kagaku Model US-9 Transparent [15], biopsyjny fantom piersi Model 052A firmy CIRS [12], drutowy obiekt testujący [12]

12.3. Measurements

12.3.1. Configurations and measuring variants

In this study, the transmitted pulses (Fig. 6a,b) and reflective signals (Fig. 6c) were recorded in the setup of the ultrasound tomography model (Fig. 1), using an ultrasonic ring array. Measurements were carried out in the water without phantom/object (Fig. 6a) and with appropriate phantom/object (Fig. 6b,c), in 3 variants for UTT transmission mode (Fig. 6a,b) and 2 variants for URT reflection mode (Fig. 6c).

In the first variant of the UTT mode (Fig. 6a,b) the ultrasonic signal generated by the selected transducer of the ring tomography array was passed through the diameter of the array (in water without and with phantom respectively), registering it with the opposite transducer. In the second variant of the UTT mode (Fig. 6a), the ultrasonic signal generated by the selected transducer of the ring tomography array was passed through the extreme chord for this mode (only in water without phantom), registering it with the transducer located at an angle of 45º to the transmitter. In the third variant of the UTT mode (Fig. 6b), the ultrasonic signal generated

by the selected transducer of the ring tomography array was passed through the measuring chord of the array, tangential to the edge of the phantom (only in water with phantom), recording it with a transducer suitable for this chord. In the first variant of the URT mode (Fig. 6c), an ultrasonic signal was emitted from the selected transducer of the ring tomography array (in water with phantom/object), registering the scattered echo signal using the same transducer. In the second variant of the URT mode (Fig. 6c), an ultrasonic signal was emitted from a selected transducer of the ring array (in water with phantom/object), recording the scattered echo signal with the use of an extreme receiving transducer for this measurement variant.

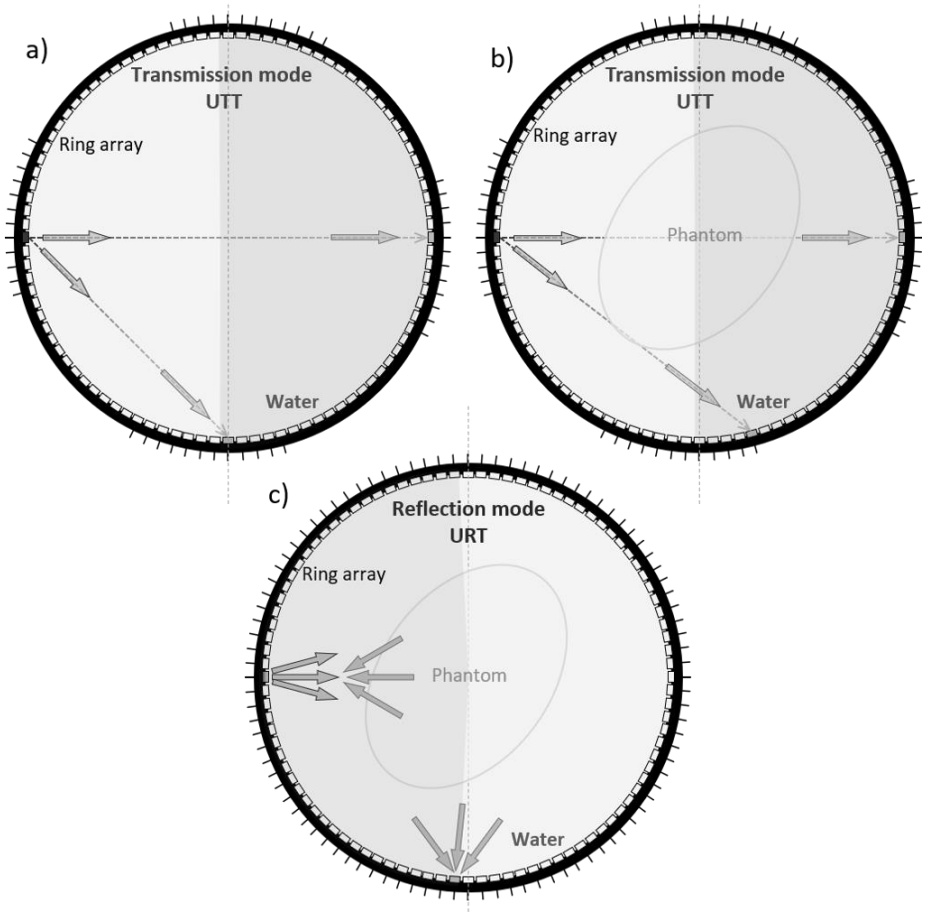

Fig. 6. The way of recording transmitted pulses and reflected signals in the setup of the ultrasound tomography model with a ring array: for the transmission mode (UTT) in water without a phantom (a), for the transmission mode (UTT) in water with a phantom (b), for the reflection mode (URT) in water with a phantom/object (c)

Rys. 6. Sposób rejestracji transmitowanych impulsów i sygnałów odbiciowych w układzie modelu tomografu ultradźwiękowego z głowicą pierścieniową: dla modu transmisyjnego (UTT) w wodzie bez fantomu (a), dla modu transmisyjnego (UTT) w wodzie z fantomem (b), dla modu odbiciowego (URT) w wodzie z fantomem/obiektem (c)

The presented measuring test variants for receiving transducers in the transmitter axis and at an angle of about 45º were selected because, in the case of tomographic measurements with

a ring array, the recorded signal is weakened not only as a result of the specific directivity of transducers in the horizontal plane but also as a result of the unevenness of transmitter and receiver pairs, which is the greater the angle between the transmitter-receiver axis and the ring diameter of the array. The level of such weakness was measured for the UGP-2 ring array [16] used in the ultrasound tomography model setup (Fig. 1), whose interior was filled with distilled water (Fig. 7).

In the ultrasound tomography array, the amplitude of the signal transmitted from a single transmitter to the receiving transducers located at an angle of ±45° to it (extreme measurements for UTT) decreases by a maximum of about 10 ÷ 12 dB concerning the amplitude from the receiving transducer located opposite the transmitter. Moreover, this decrease in the range 0 ÷ 45° (and symmetrically in the range 0 ÷ -45°) is approximately linear on a logarithmic scale, with an inclination of approximately 0.267 dB/°.

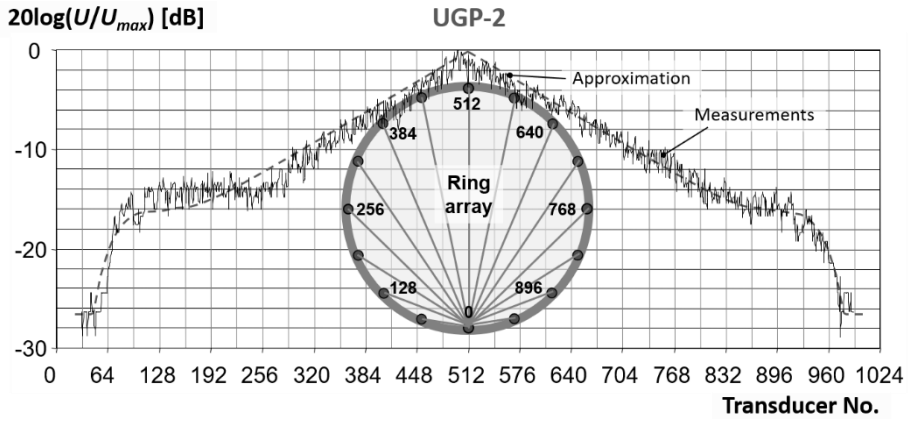

Fig. 7. The measured level of signal weakening due to unevenness of transmitter and receiver pairs of the UGP-2 ultrasonic ring array [16] used in the ultrasound tomography model setup (Fig. 1)

Rys. 7. Zmierzony poziom osłabienia sygnału w wyniku nierównoległości par przetworników nadawczych i odbiorczych ultradźwiękowej głowicy pierścieniowej UGP-2 [16] wykorzystywanej w układzie modelu tomografu ultradźwiękowego (Rys. 1)

The directivity pattern of the elementary piezoelectric transducer of the ultrasonic ring array working pulsed at $f \approx 2$ MHz is shown in Fig. 8. The angle of beam divergence for a 3 dB drop in signal amplitude to the signal on the transducer axis is 86º.

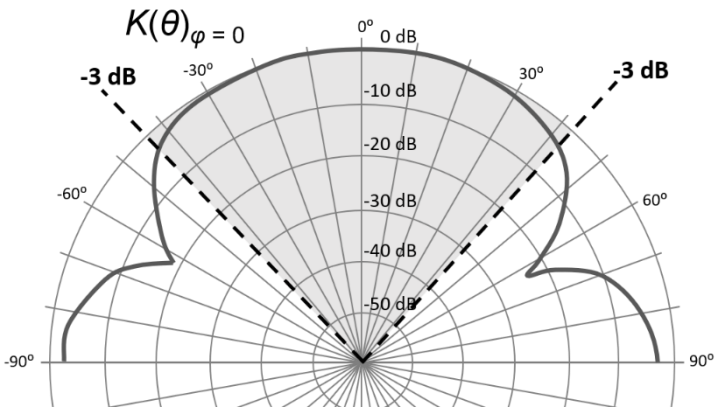

Fig. 8. Directivity pattern of the elementary ultrasonic transducer of the ring array in the horizontal plane *XOZ* in the far-field, working pulsed ($f_r \approx 2$ MHz)

Rys. 8. Charakterystyka kierunkowości elementarnego przetwornika ultradźwiękowej głowicy pierścieniowej w płaszczyźnie horyzontalnej *XOZ* w polu dalekim, pracującego impulsowo ($f_r \approx 2$ MHz)

12.3.2. Results of transmission measurements

Figure 9 shows the uncoded pulse (Fig. 2a), transmitted in 3 previously described variants for the transmission mode (UTT) by water, agar phantom, and Kyoto Kagaku breast phantom respectively (Fig. 5) and recorded in the setup of the ultrasound tomography model with ring array (Fig. 1).

The signals obtained using matched filtering (chapter 2.3) of the uncoded pulse, chirp pulse, Barker code, and complementary Golay codes (Fig. 2), transmitted respectively in 3 previously described variants for the transmission mode (UTT) by water, agar phantom and Kyoto Kagaku breast phantom (Fig. 5) and recorded in the setup of the ultrasound tomography model with the ring array (Fig. 1), are presented successively in Fig. 10, Fig. 11, Fig. 12. The amplitude of pulses and signals on the *Y*-axis is presented in the steps of quantification, where 1 step corresponds to 1/256 V, amplified in the receiving amplifier with 200 V/V amplification. The duration of pulses and signals on the *X*-axis is shown in the samples for sampling frequency $f_s = 31.25$ MHz.

Analyzing the shape of signals obtained through the use of matched filtering pulses after passing through different media (Fig. 10 - Fig. 12), it can be stated that the most distorted are the signals with Barker filtering. The signals correlated with uncoded pulses have a long duration, quite long rise time, and significant fading time. Signals after matched filtering with a chirp pulse have short rise times, but are stratified - before the beginning of the pulse, there is a low-frequency, low amplitude pulse. Signals after matched filtering with Golay codes are characterized by a very short rise time and low amplitude pulse combined with the beginning of the useful pulse.

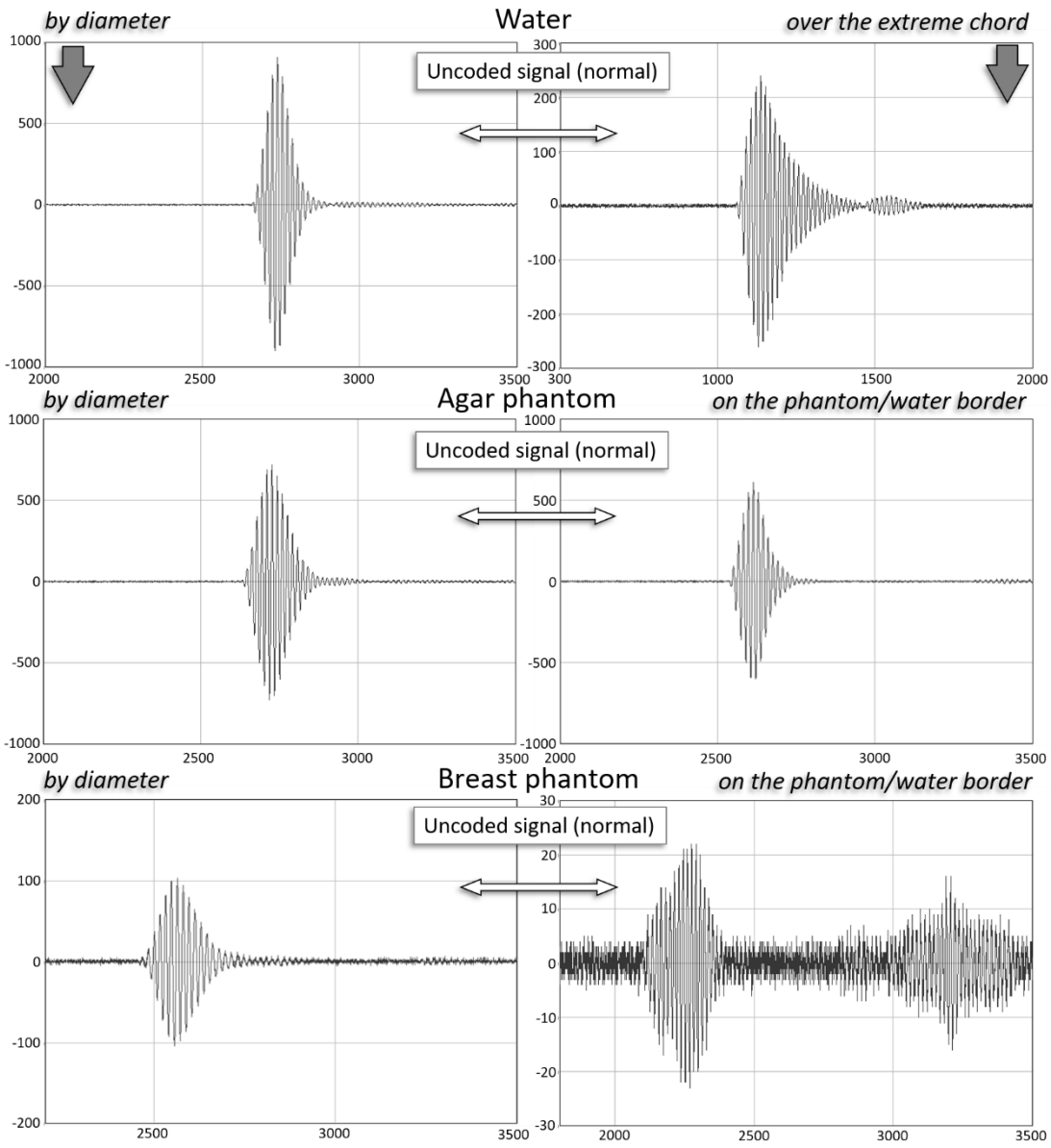

Fig. 9. Uncoded pulse (Fig. 2a) transmitted by water, agar phantom, and Kyoto Kagaku breast phantom and recorded in the setup of the ultrasound tomography model with the ring array (Y − quantization steps, X − sample number)

Rys. 9. Impuls niekodowany (rys. 2a) przetransmitowany przez wodę, fantom agarowy oraz fantom piersi Kyoto Kagaku i zarejestrowany w układzie modelu tomografu ultradźwiękowego z głowicą pierścieniową (Y – kroki kwantyzacji, X – numer próbki)

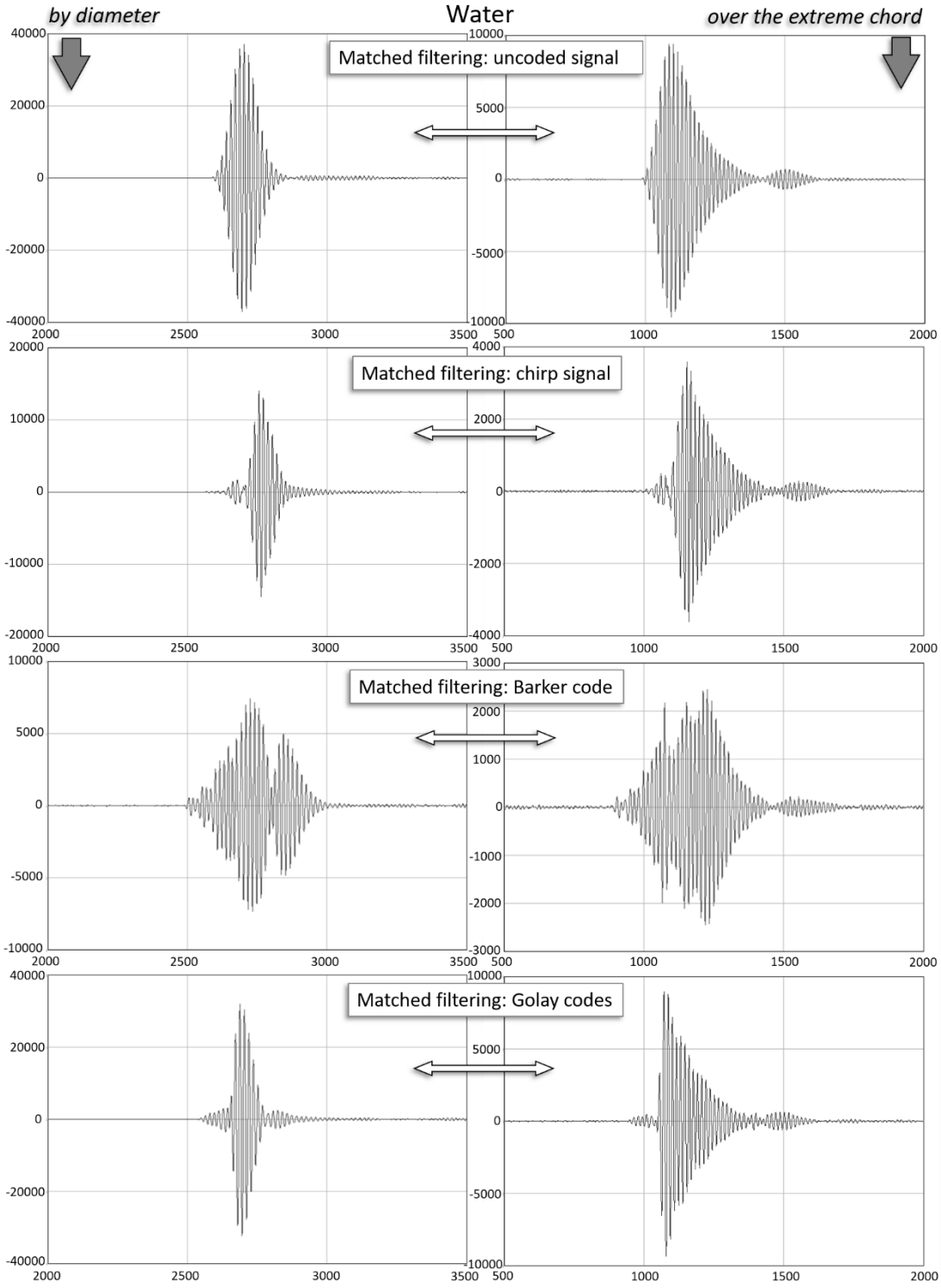

Fig. 10. Signals after matched filtering of pulses (Fig. 2) transmitted by water (Y – quantization steps, X – sample number)

Rys. 10. Sygnały po filtracji dopasowanej impulsów (rys. 2) przetransmitowanych przez wodę (Y – kroki kwantyzacji, X – numer próbki)

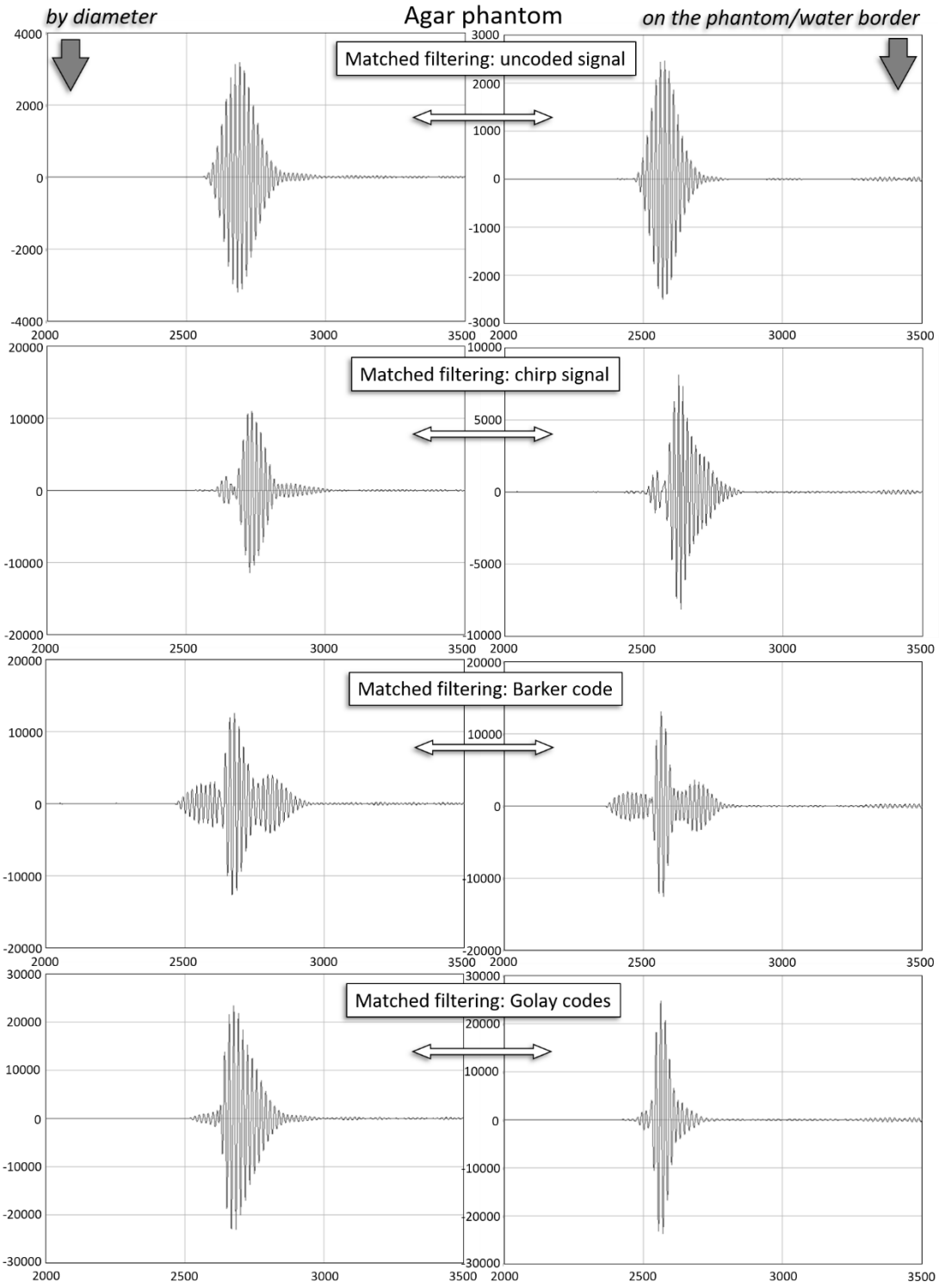

Fig. 11. Signals after matched filtering of pulses (Fig. 2) transmitted by the agar phantom (Y − quantization steps, X − sample number)

Rys. 11. Sygnały po filtracji dopasowanej impulsów (rys. 2) przetransmitowanych przez fantom agarowy (Y – kroki kwantyzacji, X – numer próbki)

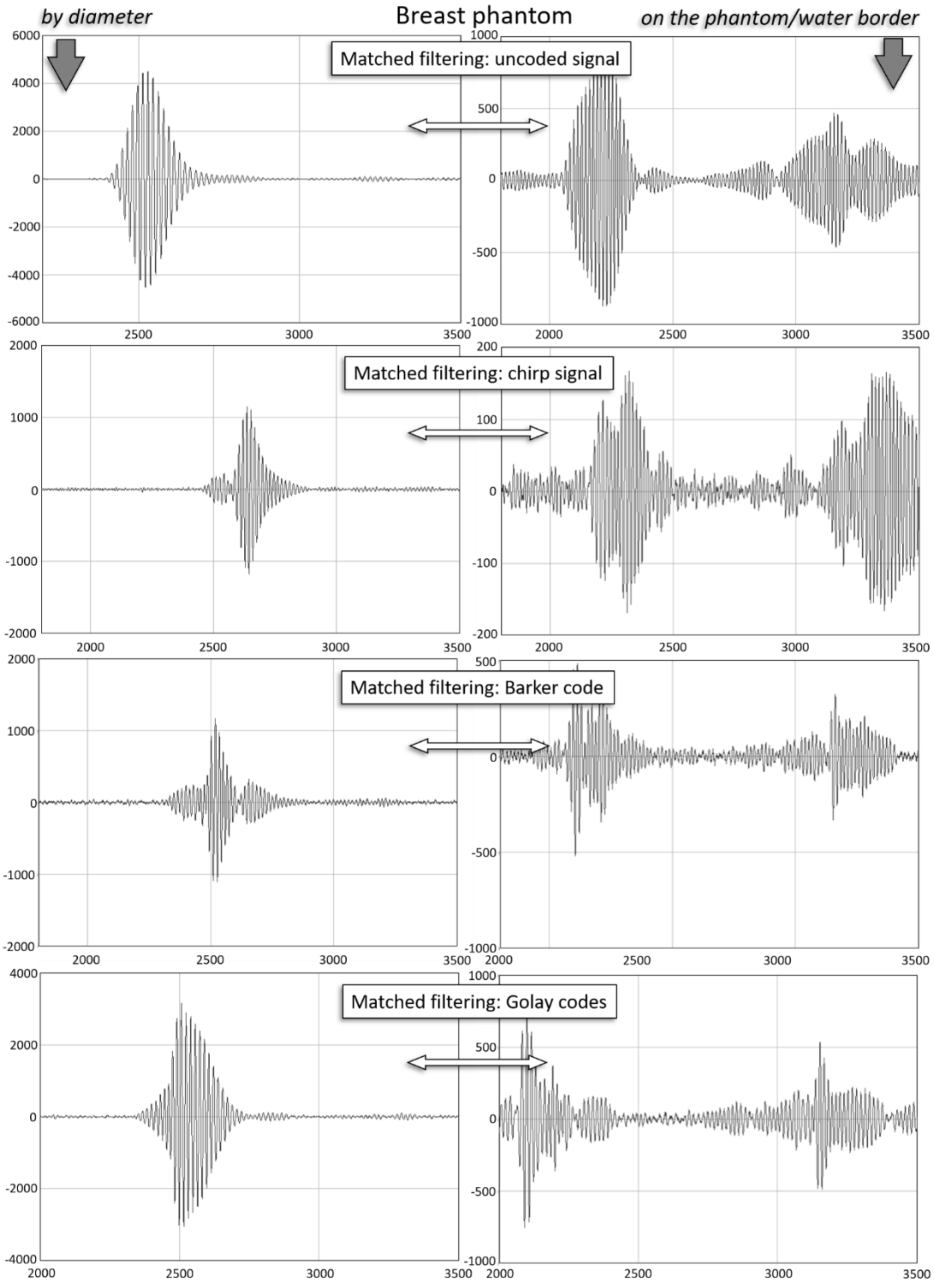

Fig. 12. Signals after matched filtering of pulses (Fig. 2) transmitted by the Kyoto Kagaku breast phantom (Y – quantization steps, X – sample number)

Rys. 12. Sygnały po filtracji dopasowanej impulsów (rys. 2) przetransmitowanych przez fantom piersi Kyoto Kagaku (Y – kroki kwantyzacji, X – numer próbki)

From the recorded envelope of pulses (Fig. 9) and signals (Fig. 10 - Fig. 12), the maximum values of useful signal and noise were determined. The values of S/N ratio levels for all pulses and signals recorded in the transmission mode are shown in Fig. 3.13 - Fig. 3.15.

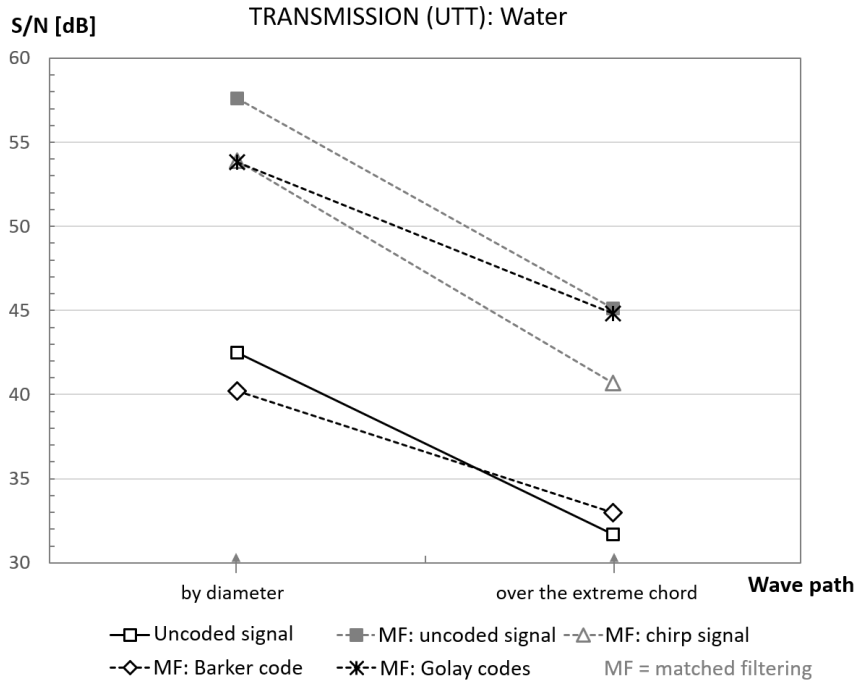

Fig. 13. Comparison of S/N levels for signal without filtering and signals after matched filtering (Fig. 2), in transmission mode, for ultrasonic wave passage through the diameter of the ring array and over its extreme chord in water

Rys. 13. Zestawienie wartości poziomów stosunku sygnału do szumu (S/N) dla sygnału bez filtracji i sygnałów po filtracji dopasowanej (rys. 2), w modzie transmisyjnym, dla przejścia fali ultradźwiękowej po średnicy głowicy pierścieniowej oraz po jej skrajnej cięciwie w wodzie

In case of pulses transmitted by water (medium with insignificant ultrasound attenuation) and signals obtained as a result of their matched filtering (Fig. 13), a decrease of S/N ratio level by about 10 - 12 dB is visible for the passage through the extreme chord of the UTT mode compared to the passage through the array diameter. This decrease results from signal weakening due to the unevenness of the transmitter and receiver pairs of the ultrasonic ring array (Fig. 7). A significant increase of S/N ratio level as a result of matched filtering was obtained here for correlation with uncoded signal (-■- *MF: uncoded signal*) by about 15 dB to standard signal (–□– *Uncoded signal*). A slightly worse result - about 10 dB was obtained for correlation with chirp signal (-Δ- *MF: chirp signal*). In the case of matched filtering with complementary Golay codes, the S/N ratio level was improved by about 10 dB for the transition on the array's diameter and about 13 dB for the transition on the extreme array's chord (- ∗- *MF: Golay codes*). Matched filtering by Barker code reduced the S/N ratio level by about 13 dB (-◊- *MF: Barker code*).

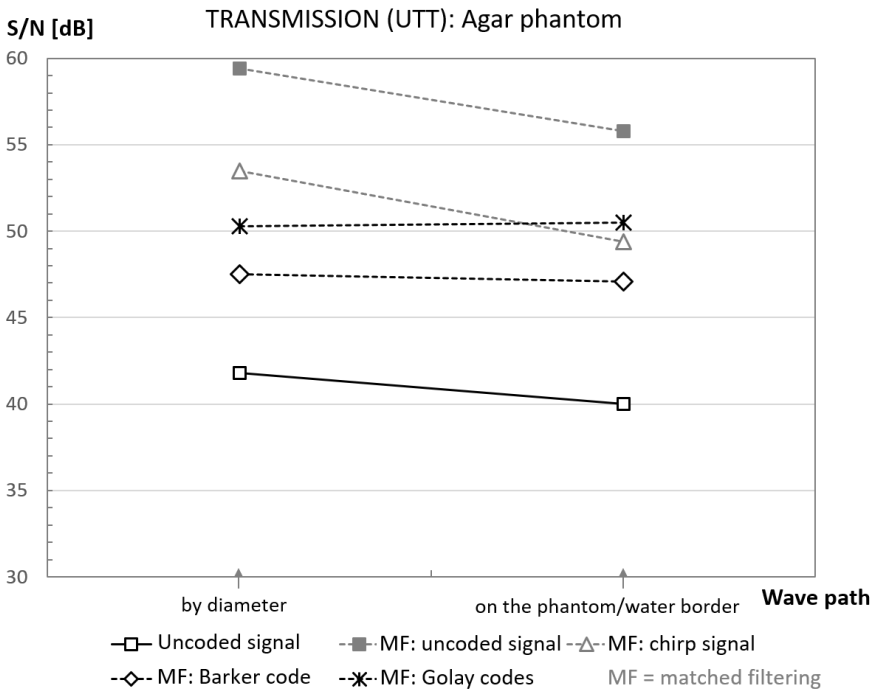

Fig. 14. Comparison of S/N ratio levels for signal without filtering and signals after matched filtering (Fig. 2), in transmission mode, for ultrasonic wave passage along the diameter of the ring array in water with agar phantom and on the phantom/water border

Rys. 14. Zestawienie wartości poziomów stosunku sygnału do szumu (S/N) dla sygnału bez filtracji i sygnałów po filtracji dopasowanej (rys. 2), w modzie transmisyjnym, dla przejścia fali ultradźwiękowej po średnicy głowicy pierścieniowej w wodzie z fantomem agarowym oraz po bocznej powierzchni fantomu

In case of pulses transmitted by the agar phantom submerged in water (medium with low ultrasound attenuation) and signals obtained as a result of their matched filtering (Fig. 14), the drop of S/N ratio level for the passage on the side edge of the phantom (on the phantom/water border) compared to the passage on the diameter of the array (phantom is placed centrally in the area of the array ring) is small and changes depending on the way the pulse is coded in the range ~0 dB for Golay code matched filtering, ~0.4 dB for Barker code matched filtering, ~3.5 dB for standard signal matched filtering, ~4 dB for chirp signal matched filtering. A significant increase in the S/N ratio level as a result of the matched filtering was obtained here for the correlation with the uncoded signal (-■- *MF: uncoded signal*) by about 18 dB compared to the standard signal (–□– *Uncoded signal*). A slightly worse result - about 12 dB was obtained for a correlation with the chirp pulse (-Δ- *MF: chirp signal*), for the matched filtering with Golay codes about 8 dB (-∗- *MF: Golay codes*) and for a correlation with the Barker code about 6 dB (-◊- *MF: Barker code*).

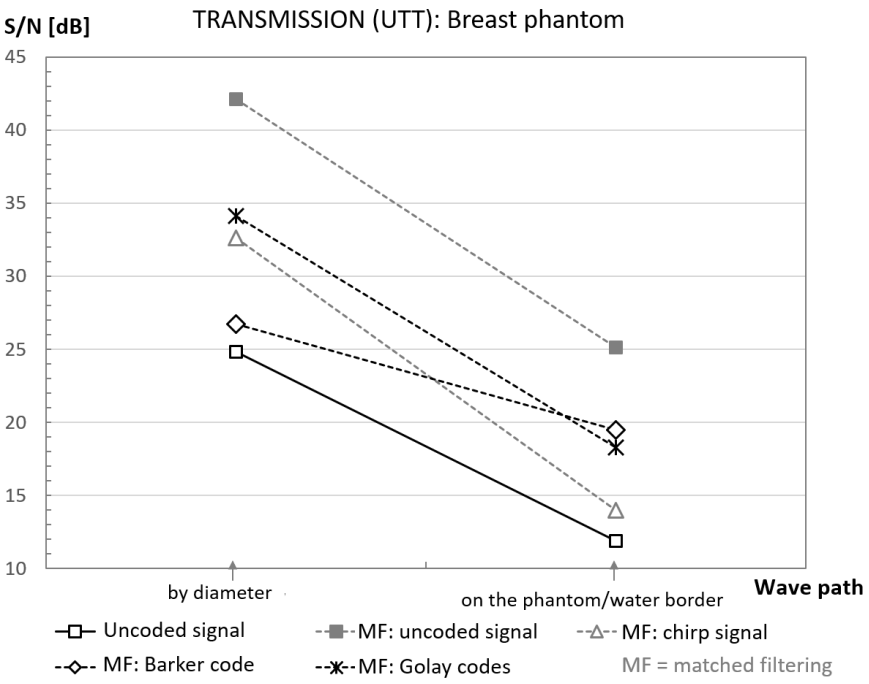

Fig. 15. Comparison of S/N ratio levels for signal without filtering and signals after matched filtering (Fig. 2), in transmission mode, for ultrasonic wave passage along the diameter of the ring array in water with Kyoto Kagaku breast phantom and on the phantom/water border

Rys. 15. Zestawienie wartości poziomów stosunku sygnału do szumu (S/N) dla sygnału bez filtracji i sygnałów po filtracji dopasowanej (rys. 2), w modzie transmisyjnym, dla przejścia fali ultradźwiękowej po średnicy głowicy pierścieniowej w wodzie z fantomem piersi Kyoto Kagaku oraz po bocznej powierzchni fantomu

In case of pulses transmitted by the Kyoto Kagaku breast phantom submerged in water (medium with high ultrasound attenuation) and signals obtained as a result of their matched filtering (Fig. 15), the decrease of S/N ratio level for the passage on the side edge of the phantom (on the phantom/water border) compared to the passage on the diameter of the array (the phantom is placed centrally in the area of the array ring) is about 5 dB for the correlation with the Barker pulse (-◊- *MF: Barker code*) and about 11 - 19 dB for the remaining signals. A significant increase in the S/N ratio level as a result of matched filtering was obtained here for the correlation with the uncoded signal (- ■ - *MF: uncoded signal*) by about 17 dB compared to the standard signal (–□– *Uncoded signal*). A worse result - about 10 dB was obtained for the matched filtering with Golay codes (-∗- *MF: Golay codes*) and about 8 dB for the correlation with the chirp signal (-Δ- *MF: chirp signal*). A slight increase in S/N was obtained for correlation with the Barker pulse (-◊- *MF: Barker code*) for diameter transition (~2 dB) and four times the increase for phantom edge transition (~8 dB).

12.3.3. Results of reflection measurements

The signals and their envelopes recorded in the ultrasound tomography setup with the ring array (Fig. 1) (without filtration and with matched filtering) dispersed in submerged in water cross-section of the agar phantom and the Kyoto Kagaku breast phantom (Fig. 5) are presented in Fig. 16 – Fig. 17 respectively in the URT mode first variant described earlier (Fig. 6). The amplitude of pulses and signals on the *Y*-axis is presented in quantization steps, where 1 step corresponds to 1/256 V, amplified in the receiving amplifier with 200 V/V amplification. The duration of pulses and signals on the *X*-axis is shown in the samples for sampling frequency f_s = 31.25 MHz.

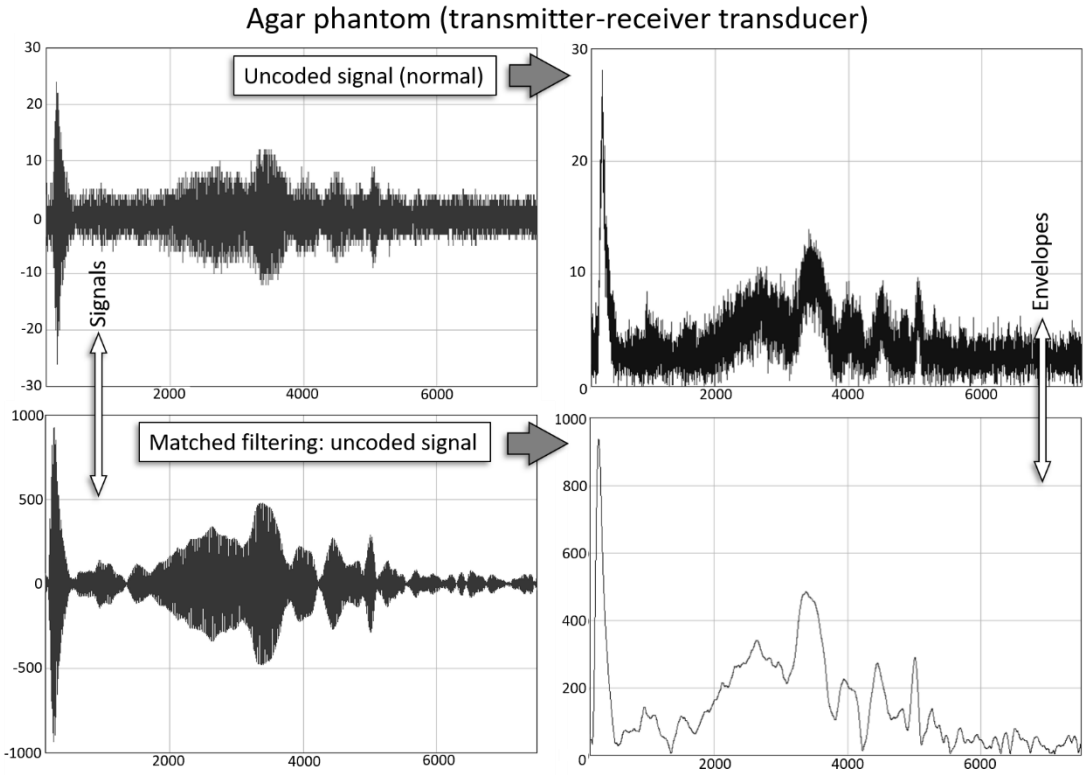

Fig. 16. Backscattered uncoded signal (normal) and its envelope in the cross-section of the agar phantom submerged in water: in the upper line – without filtration, in the lower line – after matched filtering; transmitting and receiving from the same ring array transducer (*Y* − quantization steps, *X* − sample number)

Rys. 16. Sygnał rozproszony (normalny) w przekroju fantomu agarowego zanurzonego w wodzie oraz jego obwiednia: w górnym wierszu − bez filtracji, w dolnym wierszu – po filtracji dopasowanej; nadawanie i odbiór z tego samego przetwornika głowicy pierścieniowej (*Y* – kroki kwantyzacji, *X* – numer próbki)

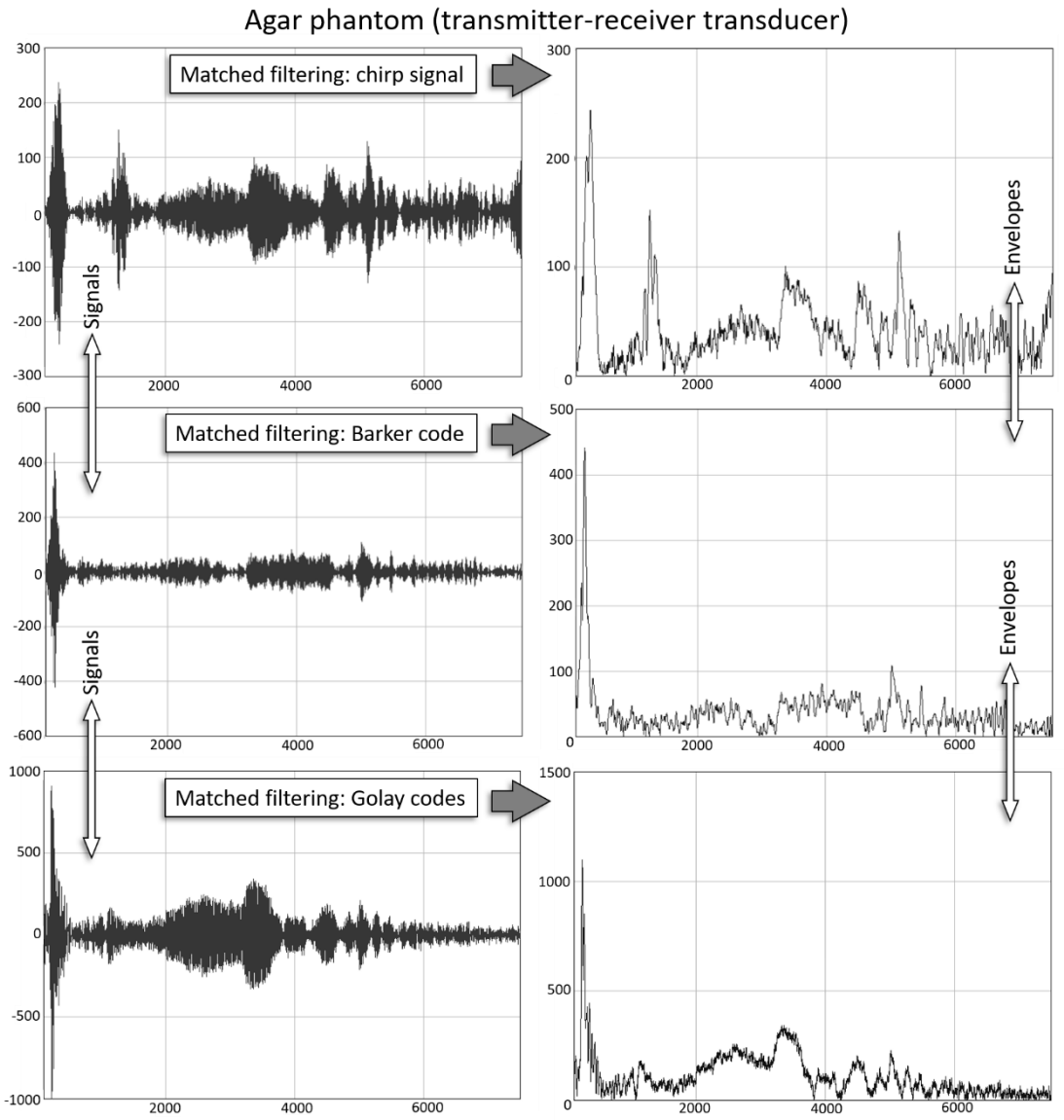

Fig. 17. Backscattered signals (in the left column) in the cross-section of the agar phantom submerged in water and their envelope (in the right column), after matching filtering; transmitting and receiving from the same ring array transducer (Y − quantization steps, X − sample number)

Rys. 17. Sygnały rozproszone (w lewej kolumnie) w przekroju fantomu agarowego zanurzonego w wodzie oraz ich obwiednie (w prawej kolumnie), po filtracji dopasowanej; nadawanie i odbiór z tego samego przetwornika głowicy pierścieniowej (Y – kroki kwantyzacji, X – numer próbki)

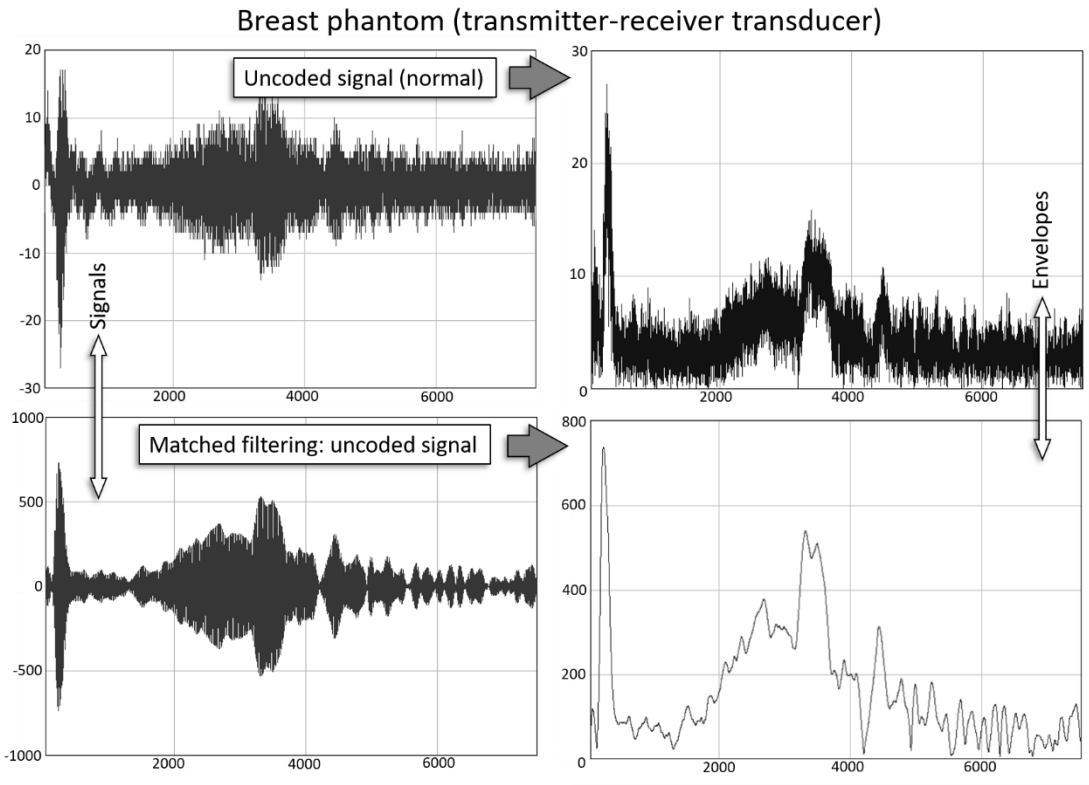

Fig. 18. Backscattered signal (normal) and its envelope in the cross-section of the Kyoto Kagaku breast phantom submerged in water: in the upper line − without filtering, in the lower line – after matching filtering; transmitting and receiving from the same ring array transducer (Y − quantization steps, X − sample number)

Rys. 18. Sygnał rozproszony (normalny) w przekroju fantomu piersi Kyoto Kagaku zanurzonego w wodzie oraz jego obwiednia: w górnym wierszu − bez filtracji, w dolnym wierszu – po filtracji dopasowanej; nadawanie i odbiór z tego samego przetwornika głowicy pierścieniowej (Y – kroki kwantyzacji, X – numer próbki)

In the case of transmission and reception realized by the same central transducer of the URT sequence, a very large number of overlapping echoes is recorded as a result of backscattering of ultrasonic pulses (Fig. 16 - Fig. 19). In the case of the transmission of the URT sequence realized by the central transducer and the reception realized by the extreme transducer, the transmitting pulse is primarily received by that transducer, and the backscattering is small due to its lateral position (at an angle close to 90º) to the sending transducer. For this reason, the signals recorded in the second variant (Fig. 6) for the URT mode are not presented in this paper.

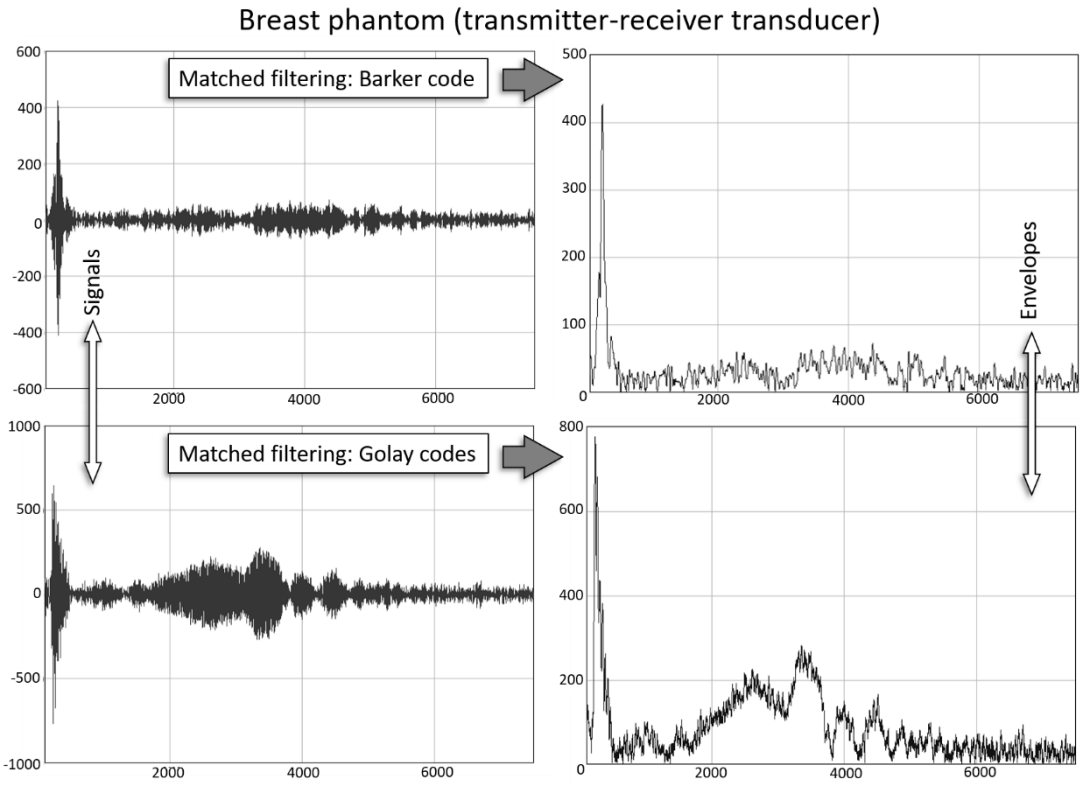

Fig. 19. Backscattered signals (in the left column) in the cross-section of the Kyoto Kagaku breast phantom submerged in water and their envelope (in the right column), after matching filtering; transmitting and receiving from the same ring array transducer (Y − quantization steps, X − sample number)

Rys. 19. Sygnały rozproszone (w lewej kolumnie) w przekroju fantomu piersi Kyoto Kagaku zanurzonego w wodzie oraz ich obwiednie (w prawej kolumnie), po filtracji dopasowanej; nadawanie i odbiór z tego samego przetwornika głowicy pierścieniowej (Y – kroki kwantyzacji, X – numer próbki)

With the use of transmitter-receiver transducer, the reflective signal obtains large amplitudes after the matched filtering with the use of uncoded pulse (Fig. 16, Fig. 18), as well as after the matched filtering with the use of complementary Golay codes (Fig. 17, Fig. 19), but after the matched filtering with the use of uncoded pulse, the signal is the smoothest (Fig. 16, Fig. 18), and the individual echoes have a long duration, rise, and fall (similarly to the matched filtering with the use of complementary Golay codes - Fig. 17, Fig. 19). The type of phantom did not significantly affect the differentiation of the reflected signals (compare Fig. 16 with Fig. 18 and Fig. 17 - Fig. 19).

From the recorded envelopes of reflective signals, the maximum values of useful signal and noise were determined. The values of S/N ratio levels for all the signals recorded in the reflection mode are presented in Fig. 20 for measurements of the agar phantom and in Fig. 21 for measurements of the Kyoto Kagaku breast phantom. For some signals a fragment of noise could not be found - in such cases S/N values were not marked on the graphs (no lines).

Fig. 20. Comparison of S/N ratio levels for signals scattered in the cross-section of the agar phantom submerged in water, without filtering and after matched filtering, in reflection mode, with transmitting and receiving from the same transducer

Rys. 20. Zestawienie wartości poziomów stosunku sygnału do szumu (S/N) dla sygnałów rozproszonych w przekroju zanurzonego w wodzie fantomu agarowego bez filtracji i po filtracji dopasowanej, w modzie odbiciowym, przy nadawaniu i odbiorze z tego samego przetwornika

In reflection measurements, with the use of transmitter-receiver transducer, an increase of S/N ratio was obtained to unfiltered echo signal from the uncoded pulse stimulus (–□– *Uncoded signal*) by: about 4 dB for the signal after the chirp matched filtering (-Δ- *MF: chirp signal*), about 7 dB for the signal after the uncoded pulse matched filtering (-■- *MF: uncoded signal*) (Fig. 20), about 10 dB for the signal after filtering with Barker code (-◊- *MF: Barker code*) (Fig. 21). For filtering with complementary Golay codes (-∗- *MF: Golay codes*), we observe the extraction of useful echoes of the receiving signal not previously seen in noise (Fig. 17, Fig. 19). In this case, it was not possible to determine the S/N ratio level, because no part of the signal that could be considered as noise without diffuse echoes was found.

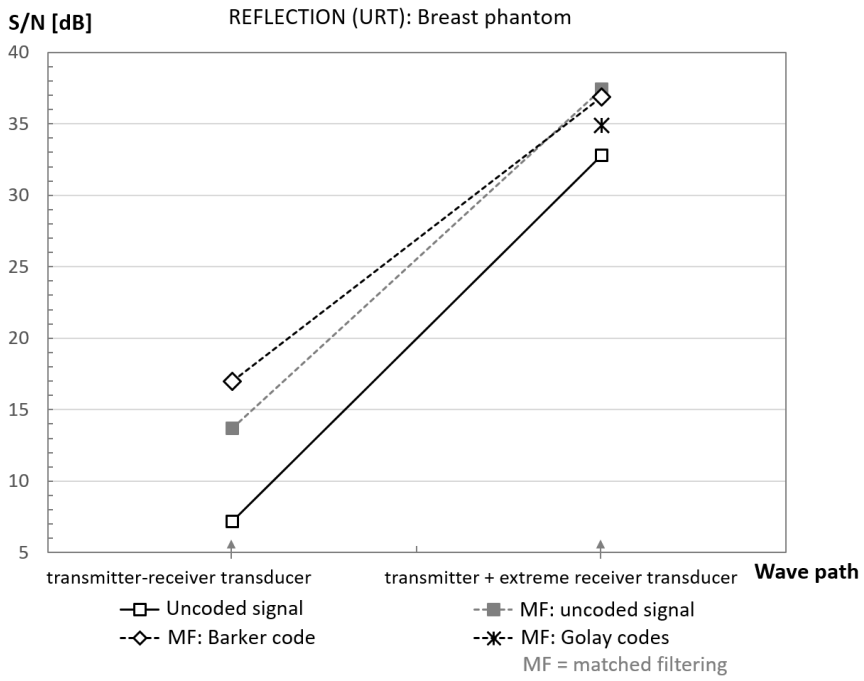

Fig. 21. Comparison of S/N ratio levels for signals backscattered in the cross-section of the Kyoto Kagaku breast phantom submerged in water, without filtering and after matched filtering, in reflection mode, with transmitting and receiving from the same transducer

Rys. 21. Zestawienie wartości poziomów stosunku sygnału do szumu (S/N) dla sygnałów rozproszonych w przekroju zanurzonego w wodzie fantomu piersi Kyoto Kagaku bez filtracji i po filtracji dopasowanej, w modzie odbiciowym, przy nadawaniu i odbiorze z tego samego przetwornika

In reflection measurements, with transmission from the central transducer and reception from the extreme transducer, an increase in S/N was obtained to the unfiltered echo signal from the uncoded stimulus (–□– *Uncoded signal*) by about 23 dB for the signal after matched filtering using the uncoded pulse (-■- *MF: uncoded signal*) in the agar phantom (Fig. 20) and about 5 dB in the breast phantom (Fig. 21), 13 - 15 dB for the signal after matched filtering with chirp pulse (-Δ- *MF: chirp signal*) and Barker code (-◊- *MF: Barker code*) in the agar phantom (Fig. 20) and about 4 dB for the signal after matched filtering with Barker code (-◊- *MF: Barker code*) in the breast phantom (Fig.21), about 7 dB for the signal after matched filtering with complementary Golay codes in the agar phantom (Fig. 20) and about 2 dB in the breast phantom (Fig. 21). When transmitting a URT sequence from the central transducer and receiving from the extreme transducer, the transmitting pulse is mainly transmitted to that transducer by the shortest route - by a chord connecting both transducers and deviating from the wave propagation axis by about 45º. Therefore, the backscattering is negligible here - the transmission pulse dominates the reflection signal. This pulse is the widest (in terms of duration), has the highest amplitude, and is the smoothest after the matched filtering with the uncoded pulse. Matched filtering with Barker and Golay codes shortens the pulse, but introduces additional low amplitude parasitic pulses at its beginning, similar to the transmission mode (Fig. 10 - Fig. 12).

It is characteristic that transmission signals and echoes in the reflection signal move as a result of this phenomenon towards smaller values on the timeline in a non-linear way. The summation of parasitic pulses shifted in the phase results in the creation of additional maxima in the signal, which makes it difficult to precisely determine the amplitude and time of the passage of the pulse despite the increase in S/N ratio level.

12.3.4. Examples of UTT and URT imaging results using coded pulses

The shifting of echoes and pulses, the creation of additional maxima in the coded tomographic signals processed by the matched filtering method results in the appearance of artifacts and distortions in the reconstructed ultrasound tomography images (especially transmission ones). At this stage of research, it is therefore only possible to present exemplary imaging results using signal coding and the use of transition time and amplitude detection algorithms developed for uncoded signals. In the case of coded signals, more extensive research would have to be done to find an appropriate modification of the detection algorithms, which would significantly extend beyond the range of current research. Examples of results of CIRS Model 052A breast biopsy phantom imaging and wire testing object (Fig. 5) using signal coding but together with signal detection algorithms of transition times and amplitudes of ultrasound signals developed for uncoded signals are presented in Fig. 22 and Fig. 23, respectively.

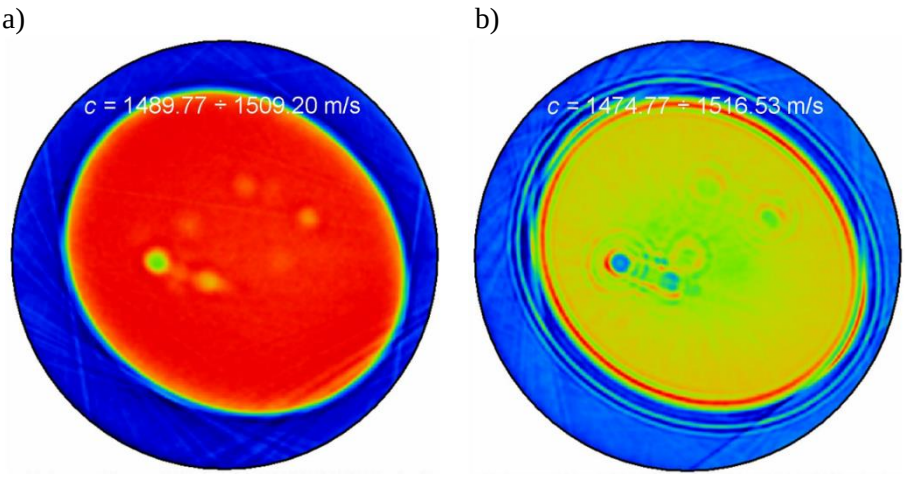

Fig. 22. Exemplary, comparative results of UTT imaging cross-section of the CIRS Biopsy Model 052A breast phantom (Fig. 5) − distribution of local ultrasound speed values: a) without signal coding and without matched filtering, b) using Barker code and matched filtering

Fig. 22. Przykładowe, porównawcze wyniki ultradźwiękowego transmisyjnego obrazowania tomograficznego przekroju biopsyjnego fantomu piersi Model 052A firmy CIRS (rys. 5) – rozkład lokalnych wartości prędkości ultradźwięków: a) bez kodowania sygnału i bez filtracji dopasowanej, b) z zastosowaniem kodu Barkera i filtracji dopasowanej

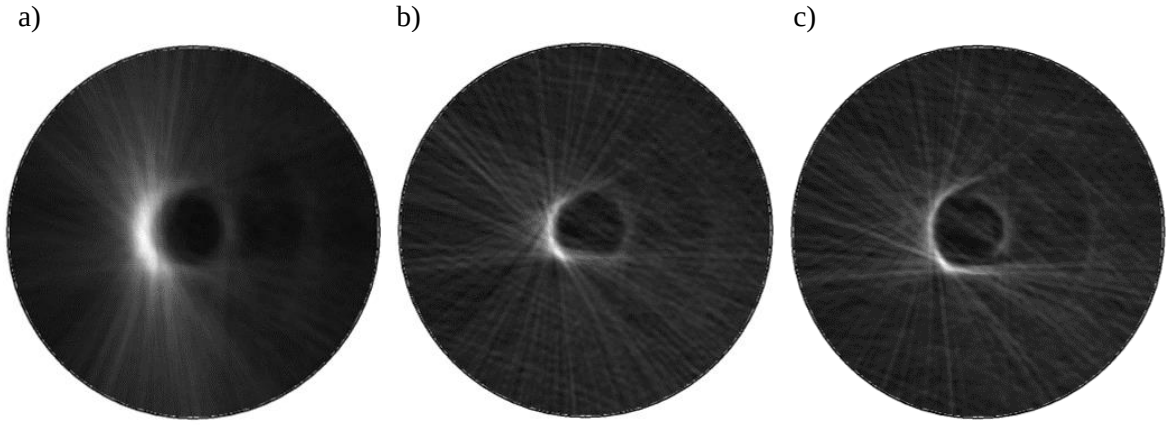

Fig. 23. Exemplary, comparative results of URT imaging cross-section of one wire element of the wire testing object (Fig. 5) − distribution of relative values of the ultrasound scattering coefficient: a) without signal coding and matched filtering, b) with matched filtering with normal transmitting signal, c) with matching filtering with complementary Golay codes

Rys. 23. Przykładowe, porównawcze wyniki ultradźwiękowego odbiciowego obrazowania tomograficznego przekroju jednego elementu drutowego obiektu testującego (rys. 5) – rozkład względnych wartości współczynnika rozpraszania ultradźwięków: a) bez kodowania sygnału i bez filtracji dopasowanej, b) z zastosowaniem filtracji dopasowanej z normalnym sygnałem nadawczym, c) z zastosowaniem filtracji dopasowanej z komplementarnymi kodami Golaya

In the case of the transmission mode (UTT), the use of pulse coding sharpened the heterogeneity borders and increased S/N ratio in the image, with the simultaneous introduction of artifacts – additional artificial borders in the form of multiple halos with significantly increased ultrasound speed (Fig. 22). This is a result of additional maxima in the signal. Moving the pulses after matched filtering also leads to the falsification of the reconstructed ultrasound speed values and falsification of the shape and position of heterogeneities.

In the case of reflection mode (URT), the use of pulse coding has resulted in a significant sharpening of the heterogeneity borders with an increase in imaging dynamics (Fig. 23). The artifacts here are mainly related to the falsification of the heterogeneity shape as a result of shifting echoes in the signals after matched filtering.

12.4. Summary and conclusions

Summarizing the detailed research carried out in this paper on the possibility of using linear frequency modulation and discrete phase modulation with algebraic codes in ultrasound transmission and reflection tomography of the breast it can be stated that:

a) with limited relative bandwidth of ultrasonic transducers, below 25%, significant distortions of coding sequences occur which are generated in water and tissue,
b) with limited relative bandwidth of ultrasonic transducers, the use of matched filtering in the form of signal correlation with the normal transmission pulse for use in URT may be

considered; such correlation increases the S/N ratio level and increases the imaging resolution,

c) with limited relative bandwidth of ultrasonic transducers, despite a significant increase in S/N and image sharpening, the use of signal coding in UTT introduces artifacts into reconstructed images,

d) it is possible to achieve improved dynamics and resolution of imaging and elimination of artifacts in transmission and reflection imaging as a result of signal coding for a wide relative bandwidth of ultrasonic transducers, above 70%.

The measurements carried out in this work were performed using one of the first models of UGP-2 ultrasonic ring array with parameters: f_r = 1.96 MHz, B = 0.25 MHz, $Q \approx 8$; $B_w = (\Delta f/f_r)\cdot 100\% \approx 13\%$. The newest model of the ring array, thanks to the well-optimized front matching layer, is characterized by a significantly extended band of ultrasonic transducers: f_r = 2 MHz, B = 1.5 MHz, $Q \approx 1.33$; $B_w \approx 75\%$. Due to the very wide bandwidth of the UGP-X array model, it seems possible to use here the coding of signals which will not be distorted both in transmission and reflection mode. Due to the short patient examination time *in vivo*, it would be advisable to use the coding of signals with single emission - e.g. Barker code. Such coding can also be successfully used in the currently tested omnidirectional standard ultrasound B-mode imaging [17] performed with a ring array in the ultrasound tomography prototype.

It should be noted that dual transmitting of a complementary pair of Golay codes is associated with a doubling of signal acquisition time and double time compression. Any movement of the imaged object (breast tissue *in vivo*) between subsequent transmissions causes the appearance of side lobes resulting from the decorrelation between the received signals. The reduction of the transmission time of complementary Golay codes could be achieved by transmitting two complementary codes simultaneously using two transducer apertures [18]. In the receiving signals, it is later possible to separate the sequences for both codes. In the process of matched filtering the receiving signals for the complementary Golay A and B codes, it is possible to perform the convolution operation directly with the transmitted Golay signals instead of correlating them with the signals reversed in time. The use of correlation with the matched filter allows the use of programmable filters for this purpose, which can be implemented in FPGA electronics. On the other hand, the use of convolution operation allows for quick realization of this operation in digital circuits in the Fourier field by multiplying FFT transforms.

It results from the conducted works that the use of signal coding in the UTT and URT mode requires additional studies on the influence of signal coding on imaging with modification of algorithms for detection of acoustic parameters, which are currently adapted to uncoded signals.

Bibliography

1. Nowicki A.: Ultradźwięki w medycynie – wprowadzenie do współczesnej ultrasonografii. Wydawnictwo Instytutu Podstawowych Problemów Techniki, PAN, Warszawa 2010 [in Polish].
2. Nowicki A.: Ultrasonografia – wprowadzenie do obrazowania i metod dopplerowskich. Wydawnictwo Instytutu Podstawowych Problemów Techniki, PAN, Warszawa 2016 [in Polish].
3. Bilgutay N.M., Furgason E.S., Newhouse V.L.: Evaluation of the random signal correlation system for ultrasonic flaw detection. IEEE Trans. Sonics and Ultrasonics, SU-23(5), 1976, 329-333.
4. Furgason E.S., Newhouse V.L., Bilgutay N.M., Cooper G.R.: Application of random signal correlation techniques to ultrasonic flaw detection. Ultrasonics, 13(1), 1975, 11-17.
5. Robinson E.A., Treitel S.: Geophysical signal analysis. Englewood Cliffs, Prentice Hall, 1980.
6. Trots I., Nowicki A., Secomski W., Litniewski J.: Golay sequences – sidelobe-canceling codes for ultrasonography. Archives of Acoustics, 29(1), 2004, 87-89.
7. Lewandowski M.: Ultrasonografia kodowana: transmisja i kompresja w czasie rzeczywistym. PhD Thesis, IPPT PAN, Warszawa 2009 [in Polish].
8. Misaridis T.X., Gammelmark K., Jorgensen Ch.H., Lindberg N., Thomsen A.H., Pedersen M.H., Jensen J.A.: Potential of coded excitation in medical ultrasound imaging. Ultrasonics, 38(1-8), 2000, 183-189.
9. Opieliński K.J.: Ultradźwiękowe metody tomograficznego obrazowania piersi, [in:] Torbicz W. (ed.): Obrazowanie biomedyczne. Akademicka Oficyna Wydawnicza EXIT, Warszawa 2020, 613-642 [in Polish].
10. Zapf M., Derouiche B.F., Ruiter N.V.: Evaluation of Chirp and Binary Code based Excitation Pulses for 3D USCT. 2009 IEEE International Ultrasonics Symposium Proceedings, 20-23 September 2009, Rome, Italy.
11. Milewski T., Michalak M., Wiktorowicz A., Opieliński K., Pruchnicki P., Bułkowski M., Gielecki J. and Jóźwik M.: Hybrid Ultrasound Tomography Scanner-a Novel Instrument Designed to Examine Breast as a Breast Cancer Screening Method. Biomedical Journal of Scientific & Technical Research, 14(4), 2019, 5.
12. Opieliński, K.J., Pruchnicki, P., Gudra, T., Podgórski P., Kurcz J., Kraśnicki T., Sąsiadek M., Majewski J.: Imaging results of multi-modal ultrasound computerized tomography system designed for breast diagnosis. Computerized Medical Imaging and Graphics, 46, 2015, 83–94.
13. Klauder J.R., Price A.C., Darlington S., Albersheim W.J.: The theory and design of chirp radars. The Bell System Technical Journal, XXXIX(4), 1960, 745 - 808.
14. Golay M.J.E.: Complementary series. IRE Trans. Inf. Theory, IT-7, 1961, 82-87.

15. Kyoto Kagaku co., LTD. Ultrasound-Guided Breast Biopsy Phantom – Model US-9, 2017. https://www.kyotokagaku.com/products/detail01/us-9.html (20.10.2017).
16. Opieliński K.J., Gudra T.: Bioacoustic range equation. Hydroacoustics, 19, 2016, 307-318.
17. Sabiniok M., Opieliński K.J., Lis S.: Analysis of Using Multi-Angle Conventional Ultrasound Scanning for Efficient 3-D Object Imaging. Archives of Acoustics, 44(4), 2019, 645-657.
18. Jin Ch., Chen S., Qin Z., Wang T.: A new scheme of coded ultrasound using Golay codes. Journal of Zhejiang University-SCIENCE C (Computers & Electronics), 11(6), 2010, 476-480.

Acknowledgment

The research was carried out under the project POIR.01.01.01-00-1595/15, entitled: "Development of a prototype of multimodal ultrasound tomography for breast diagnosis", co-financed by the European Union from the European Regional Development Fund (Sub-measure 1.1.1 Industrial research and development work carried out by companies, Operational Programme Intelligent Development 2014-2020), as part of the funding granted by the National Centre for Research and Development.